

J. Einarsson · A. Johansson · S. K. Mahato · Y. N. Mishra ·
J.R. Angilella · D. Hanstorp · B. Mehlig

Periodic and aperiodic tumbling of microrods advected in a microchannel flow

Received: 24 November 2012 / Revised: 19 February 2013
© Springer-Verlag Wien 2013

Abstract We report on an experimental investigation of the tumbling of microrods in the shear flow of a microchannel (dimensions: $40\text{ mm} \times 2.5\text{ mm} \times 0.4\text{ mm}$). The rods are $20\text{--}30\text{ }\mu\text{m}$ long and their diameters are of the order of $1\text{ }\mu\text{m}$. Images of the centre-of-mass motion and the orientational dynamics of the rods are recorded using a microscope equipped with a CCD camera. A motorised microscope stage is used to track individual rods as they move along the channel. Automated image analysis determines the position and orientation of a tracked rod in each video frame. We find different behaviours, depending on the particle shape, its initial position, and orientation. First, we observe periodic as well as aperiodic tumbling. Second, the data show that different tumbling trajectories exhibit different sensitivities to external perturbations. These observations can be explained by slight asymmetries of the rods. Third, we observe that after some time, initially periodic trajectories lose their phase. We attribute this to drift of the centre of mass of the rod from one to another streamline of the channel flow.

1 Introduction

It was shown by Jeffery [11] that small axisymmetric rods in a viscous shear flow align for most of the time with the flow direction, but that their symmetry axes periodically and rapidly turn by 180° . This motion is referred to as ‘tumbling’ in the literature. Experimental studies of tumbling of particles in flows have been performed for a long time, see for example Goldsmith and Mason [7]. More recently, Kaya and Koser [12] report on an experiment analysing the tumbling of *E. coli* cells in microchannel shear flows. They characterised the tumbling by fitting periodic orientational trajectories to short experimental time series. A similar approach was adopted by Mishra et al. [13] to describe the tumbling of microrods in a microchannel flow. The periodic solutions referred to above were first obtained by Jeffery [11] and are commonly referred to as ‘Jeffery orbits’.

Hinch and Leal [10] have shown by theoretical analysis that slightly asymmetric rods also tumble, but that their orientational motion is in general not strictly periodic. Under certain circumstances, the authors predict that the orientational dynamics may be ‘doubly periodic’. Yarin et al. [20] refer to this motion as ‘quasi-periodic’. Their numerical results show that the tumbling can be chaotic [14]. In order to experimentally distinguish periodic from aperiodic tumbling due to asymmetry, it is necessary to observe long sequences of flips. A confounding factor is rotational and centre-of-mass diffusion: the centre of mass of an advected rod may diffuse to neighbouring streamlines of the flow. This causes aperiodicity. But noise can also directly affect the rotational degrees of freedom, leading to random tumbling.

J. Einarsson · A. Johansson · S. K. Mahato · Y. N. Mishra · D. Hanstorp · B. Mehlig (✉)
Department of Physics, University of Gothenburg, 412 96 Gothenburg, Sweden
E-mail: Bernhard.Mehlig@physics.gu.se

J. R. Angilella
LUSAC, Université de Caen, Cherbourg, France

In order to disentangle these effects, it is necessary to follow the orientational dynamics for many flips. The rods must therefore be tracked for long distances. To achieve this, we have improved an existing experimental set-up [13] in two ways. First, we have automated the image analysis of the empirical data. Second, with the new set-up, it is possible to periodically revert the channel flow. This allows us to record longer tumbling sequences. In an ideal experiment, the orientational dynamics is expected to retrace its trajectory upon reversal of the flow. This is a consequence of the time-reversal invariance of the Stokes equation governing low Reynolds number flow. Our set-up thus enables us to quantify the sensitivity of the observed tumbling motion to perturbations. In the following, we report and discuss experimentally observed tumbling trajectories. First, we see periodic and aperiodic tumbling. Second, different tumbling trajectories exhibit different sensitivities to external perturbations. We argue that these observations can be explained by slight asymmetries of the rods. Third, at very long times, initially periodic trajectories lose their phase. We attribute this to drift of the centre of mass of the rod from one to another streamline of the channel flow.

We conclude this introduction by briefly commenting on the relevance of the questions addressed in this paper. Jeffery's periodic tumbling solutions in shear flows form, together with orientational diffusion, the basis of many studies of the rheology of suspensions of non-spherical particles, as outlined by Hinch and Leal [9]. Brenner [3] and Petrie [16] have given overviews of the rheology of fibre suspensions and the use of Jeffery's and diffusion theory in this field. Furthermore, pattern formation by rods in random flows was investigated using Jeffery's theory by Wilkinson et al. [17] and Bezuglyy et al. [2] (see also Wilkinson et al. [18]), identifying singularities in the orientational patterns of rheoscopic suspensions, and explaining how Jeffery's periodic solutions determine rheoscopic visualisations of flows. Last but not least, the tumbling and alignment of small rods in turbulent flows has recently been intensively investigated, both experimentally, by simulations, and theoretically. We refer to the articles in this special issue of *Acta Mechanica*, as well as to Parsa et al. [15] and Wilkinson and Kennard [19], and to articles cited in these two papers. Simulations and the theoretical treatments of the tumbling of small rods in turbulent flows are based on Jeffery's equation of motion.

2 Materials and methods

2.1 Experimental methods

Particle synthesis. As in our earlier experiments [13], the polymer microrods are prepared by a liquid–liquid dispersion technique using the protocol of Alargova et al. [1]. This method produces rods with lengths of 10–100 μm , with typical aspect ratios of the order of 10:1. The resolution of the microscope does not allow us to determine whether the rods are symmetric or not, that is, whether they have perfectly circular or slightly elliptical cross-sections. Inspection under an optical microscope shows that the shorter rods are straight. Some of the longer rods are curved. In the experiments described below, rods in the shortest range of the span given above are used.

Design and fabrication of microfluidic channels. The microfluidic device used in this experiment is shown schematically in Fig. 1. The channel (40 mm long, 2.5 mm wide, and 0.4 mm deep) is produced in PDMS. The procedure is described in detail by Mishra et al. [13].

Optical system and tracking. A sketch of the experimental set-up is shown in Fig. 1. The optical set-up is based on a Nikon Eclipse Inverted Microscope. The channel is placed on a motorised stage, making it possible to track the rods over long time periods as they follow the flow in the channel. The rods are observed using a 20 \times microscope objective (NA=0.28). Images are recorded with a CCD camera (Leica DFC 350FX, Switzerland) at a frame rate of 100 frames per second. Each frame has a resolution of 348 \times 260 pixels. The size of a pixel is 1.2 μm \times 1.2 μm . As shown in Fig. 1, the rods are observed through a cover glass. Since the magnification of the microscope is only 20 \times , the thickness of the glass does not cause focal problems. The channel is illuminated through the transparent PDMS.

Figure 1 also shows the Cartesian coordinate system adopted in this paper. The x -axis is taken to lie along the flow in the channel. The y -axis lies along the optical axis of the microscope (the channel is 400 μm deep in this direction). The z -axis, finally, lies along the width of the channel (it is 2.5 mm wide). Thus, the camera plane corresponds to the x – z -plane, and the channel cross-section (Fig. 2) corresponds to the y – z -plane.

Channel flow. The microchannel flow is pressure-driven, using a syringe pump. The flow direction is periodically reverted. The flow is characterised by a very small Reynolds number. The rods are suspended in a 2:1 mixture of glycerol and water, corresponding to a kinematic viscosity of $\nu = 2 \cdot 10^{-5} \text{ m}^2/\text{s}$ [6]. The flow speed is of the order of 100 $\mu\text{m}/\text{s}$. Based on the smallest channel dimension (400 μm), this yields a Reynolds number of the order of $\text{Re} = 10^{-3}$. The Navier–Stokes equations for the incompressible flow in the channel thus

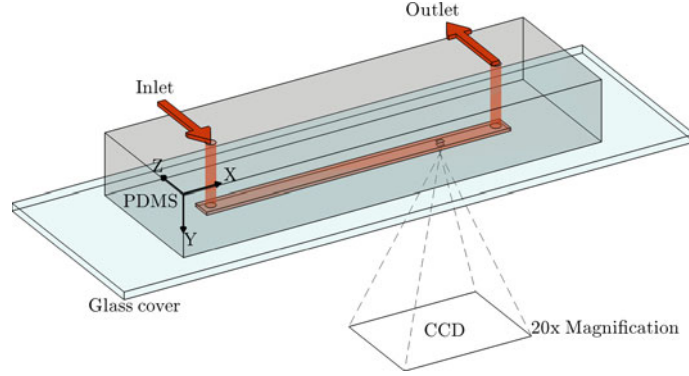


Fig. 1 Experimental set-up (schematic) with coordinate system. The microchannel is placed upon a motorised stage that allows the camera to study any part of the channel. The calculated flow rates in a cross-section of the channel are shown in Fig. 2. The coordinate system used in the analysis is shown in the figure. The origin of the coordinate system is arbitrary since only relative distances are used in the analysis

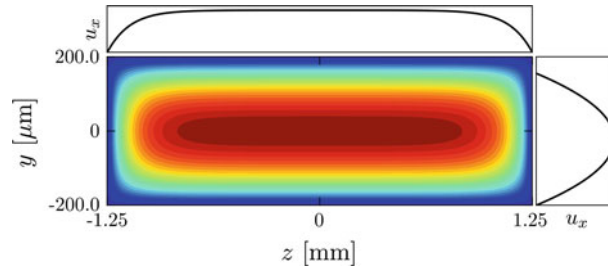


Fig. 2 Computed flow profile for the channel geometry used in experiments. The width (z) of the channel is 2.5 mm and the depth (y) is 400 μm (refer to Fig. 1 for coordinate system). The intensity plot shows a cross-section of the channel, intensity indicating flow velocity in arbitrary units. *Top* and *right* panels show the corresponding flow-velocity profiles at $y = 0$ and at $z = 0$, respectively

reduce to the viscous Stokes equation, which can be simply solved by a basis expansion. Closely following Brody et al. [4], we have computed the flow profile in a cross-section far from the in- and outlets (so that we can neglect the x -coordinate). We assume no-slip boundary conditions at the channel walls and a constant pressure gradient over the channel length. The resulting profile for our channel geometry is shown in Fig. 2. The resulting flow velocity scales as $u_x \sim \Delta p / \eta$ as a function of pressure difference Δp and dynamic viscosity η . But the form of the profile is not affected by the values of Δp or η . In Fig. 2, we observe that close to the centre of the channel, the flow gradient is oriented along the y -axis. In the following, we refer to this axis as the ‘shear direction’. The x -axis is termed ‘flow direction’ and the z -axis ‘vorticity direction’.

The rods analysed in this paper are between 20 and 30 μm long.

The viscous timescale L^2/ν is of the order of 10^{-5} s, which is much smaller than both the inverse shear rate and the flow-reversal timescale. The disturbance flow due to the inclusion is therefore expected to obey the quasi-steady Stokes equation.

2.2 Data analysis

As explained below, the rods often tumble aperiodically. Classifying different dynamical behaviours requires long time series. Since one traversal of the channel takes approximately 5 min., large amounts of data must be analysed. We have therefore designed a data analysis software (in MATLAB) to track the centre-of-mass and orientational motion of the suspended rods in an automated fashion.

The raw data from the experiment consist of time-stamped positions of the motorised stage, together with frame sequences from the microscope. The analysis uses this information to estimate time series of the centre-of-mass position of a given rod and the orientation of the unit vector \mathbf{n} along its major axis:

$$\mathbf{n} = (n_x, n_y, n_z). \quad (1)$$

The coordinate system is shown in Fig. 1.

In the remainder of this section, we briefly describe how the empirical data were processed. First, we summarise our algorithm for the image analysis. Second, we explain how time is rescaled to account for variations in the flow velocity due to reversals of the direction of the flow and due to fluctuations in the pump pressure.

2.2.1 Image analysis

The automated image analysis software tracks the centre of mass and the orientation of a given rod as it moves in the channel. We separately discuss two steps: detecting the position and orientation of the rod, and estimating its length.

Finding the rod position and orientation. To begin with, static image noise is removed as follows. For each pixel, the time-averaged intensity is computed, and for each time, the average intensity of the frame is calculated. Then, for each pixel, the time-averaged intensity is subtracted from the instantaneous intensity and the instantaneous frame average is added.

To locate the rod in a given frame, the software requires an initial guess of the centre-of-mass position. The frame rate is sufficiently high so that the tracked rods move only slightly between subsequent frames. The initial guess is therefore taken to be the last-known rod position (for the first frame, manual user input is required).

Once the location of the rod within a given frame has been estimated, a smaller window is cropped around the approximate position of the rod. An example is shown in Fig. 3a. A standard implementation of the edge-detection algorithm suggested by Canny [5] is used to find the points on the edge of a rod sufficiently contrasted from its surroundings, as shown in Fig. 3b. We estimate the rod length and its orientation starting from the set of edge pixels. To this end, we use least-squares fits to ellipses [8], because this method has proven to be less sensitive to inaccuracies in the edge detection than the commonly employed principal component analysis. These fits yield estimates of the projections of \mathbf{n} onto the camera plane (Fig. 3c). Its y -component is not directly observable, but can be computed from n_x and n_z if the length of the rod is known.

Estimating the rod length. It is impossible to determine the length of the rod from the length of its projected image in a single frame. However, the rod spends a significant amount of time aligned with the flow in the x - z -plane, where the projected length corresponds to the rod length. We therefore recorded time series of projected rod lengths and computed the distribution of projected rod lengths (Fig. 4). Ideally, the distribution should exhibit a sharp cut-off on its rhs, at the true length of the rod. However, we observe a small tail on the rhs of the distribution, caused by the experimental uncertainty of the order of one pixel size or $1.2 \mu\text{m}$. This uncertainty is indicated in Fig. 4. We therefore estimate the rod length by the position of the maximum of the distribution.

2.2.2 Time rescaling

As explained above, we revert the flow direction in order to test the sensitivity of observed orientational motion to perturbations. We have found that small perturbations may have significant effects. It is therefore important to revert the flow as smoothly as possible. This means that the flow velocity changes substantially over a significant amount of time. Another source of changes in flow speed u_x is noise in the form of uncontrolled pressure fluctuations in the pump.

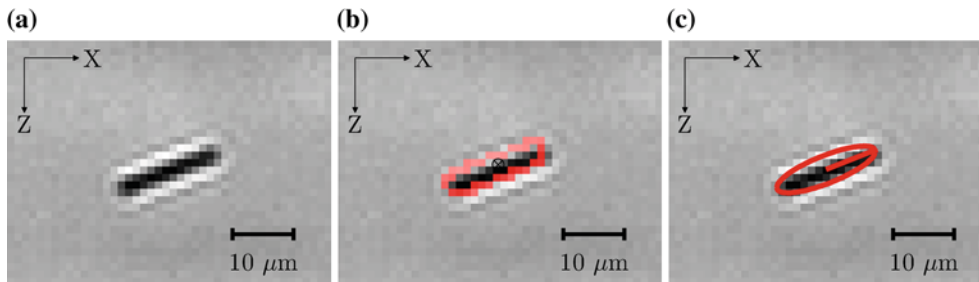


Fig. 3 Images showing a small section of output from the CCD, cropped around the approximate position of the rod. The three images illustrate three steps in the data analysis: **a** the rod is located within the video frame, **b** edges are detected with an edge-detection algorithm [5], **c** an ellipse is fitted to the resulting edge pixels. The orientation of the major axis of the ellipse is used to estimate orientation of the rod in the camera plane

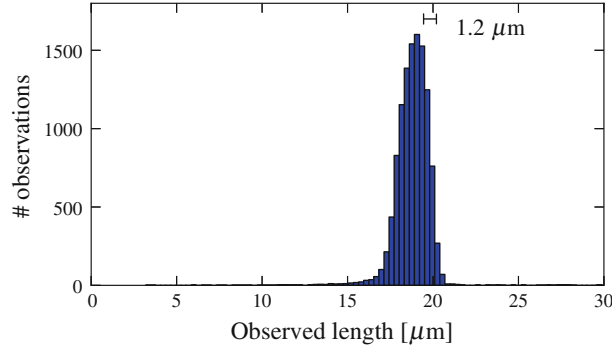


Fig. 4 A histogram of a series of measurements of the projected rod lengths in the x - z -plane of a single rod (Rod #1 in Sect. 3). The rod spends a long time nearly aligned with the flow direction. This results in the peak of the histogram. The tail to the *left* corresponds to observations when the rod is turning around, producing a shorter projection in the camera plane. The small tail to the *right* is due to the uncertainty in the measurement. The width of the tail corresponds to the size of a single pixel, indicated in the figure. The peak position is taken to be the length of the rod

But as long as the flow is governed by the linear Stokes equation (as it is in our case), the only effect of fluctuations of u_x is a linear change of timescale. To account for this change, we plot orientational trajectories as a function of distance d along the trajectory of the rod (and not as a function of time t):

$$d(t) = \int_0^t dt' u_x(t'). \quad (2)$$

The instantaneous flow velocity u_x is estimated by the centre-of-mass velocity. We assume, in other words, that the centre of mass of the rod is advected by the channel flow. The change of variables (2) greatly simplifies the analysis of our results.

3 Results

Figure 5 shows the output from the automated tracking system. The data show a long recording where the flow direction has been reversed several times by reverting the applied pressure difference. Each reversal is indicated by a vertical dotted line. The figure shows in panel (a) the relative displacement in the z -direction,

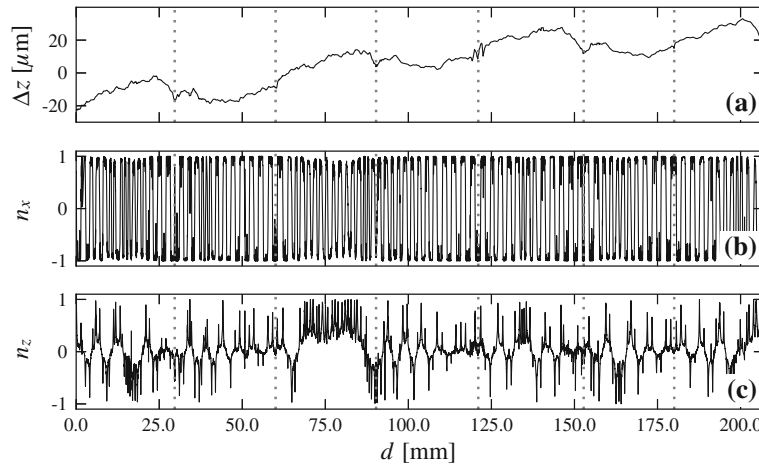


Fig. 5 Experimental output from the automated tracking system. Reversals of the flow direction are indicated by *vertical dotted lines*. **a** Relative centre-of-mass position in the x - z -plane of a rod advected in the microchannel. **b** x -component of orientation vector. **c** z -component of orientation vector

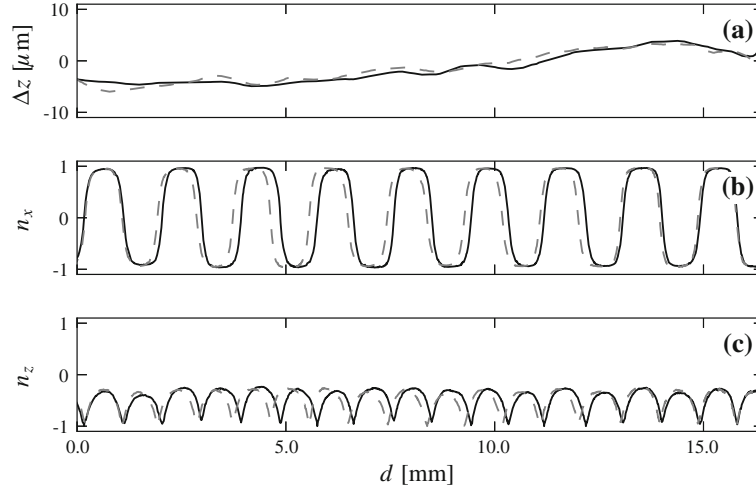


Fig. 6 **a** Fluctuations Δz of the z -coordinate of the centre-of-mass position of a rod advected in the microchannel flow from left to right (solid black line), reversed flow (dashed black line). Here, d denotes the distance covered in the x -direction, see Eq. (2). **b** x -component of orientation vector. **c** z -component of orientation vector. Rod #1 (length $19\ \mu\text{m}$, see Fig. 4)

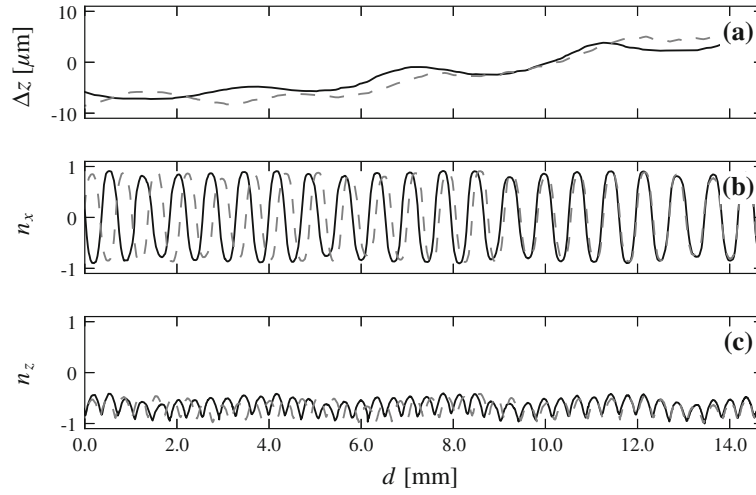


Fig. 7 Same as Fig. 6 but for rod #2 (length $22\ \mu\text{m}$)

and panels (b) and (c) show the x - and z -components of the orientation vector, all as functions of the distance the centre of mass is advected in the channel.

For a more detailed analysis of the orientational dynamics, we choose to show shorter trajectories. To measure the sensitivity of the dynamics to perturbations, we first track a given rod in one direction and record its centre-of-mass position and orientation. Then, we reverse the flow direction smoothly. In Stokes' equation, this turns u_x to $-u_x$ and, by Eq. (2), d to $-d$, effectively reversing time. In an ideal and noise-free experiment, the centre of mass and orientation are expected to retrace their trajectories. In reality, of course, and as clearly seen in Fig. 5, we observe deviations that allow us to quantify the sensitivity of the observed dynamics to perturbations.

Our results are summarised in Figs. 6, 7, and 8. The data shown in the three figures were obtained for three different rods. Each figure contains three panels: (a) a high-resolution plot of the centre-of-mass trajectory exhibiting small fluctuations Δz in the z -direction, (b) the x -component of the orientation vector, before reversal (solid line) and after reversal (dashed line), and (c) the z -component of the orientation vector.

Consider first Fig. 6. Panel (a) shows that the fluctuations Δz of the centre-of-mass trajectory are very small, only on the order of $10\ \mu\text{m}$. This is less than one rod length and is much smaller than the channel width ($2500\ \mu\text{m}$). Panel (b) shows n_x , the component of orientation vector along the flow direction. The rod spends most of its time aligned with the flow, but regularly tumbles between $n_x = 1$ and $n_x = -1$. Upon reversal, the

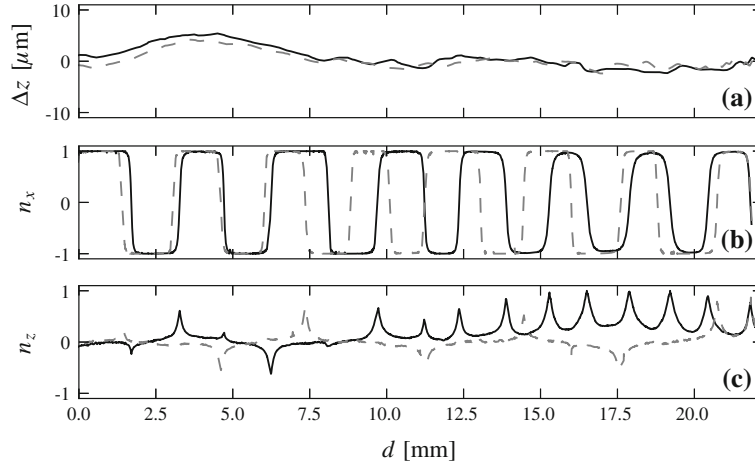


Fig. 8 Same as Fig. 6 but for rod #3 (length 30 μm)

orientational trajectory is initially similar, but drifts out of phase after several flips. The z -component of the orientation vector in panel (c) is, of course, close to $n_z = 0$ while the rod is aligned along the flow. However, during a flip, the values of n_z determine which particular orientational path the rod takes. We see that the shape of the n_z -curve during flips is similar for several subsequent flips. This indicates that the orientational trajectory is approximately periodic.

Figure 7 shows a second example. It is similar to Fig. 6, but corresponds to a different orientational trajectory. The other main difference is that the period time of the tumbling motion is shorter.

Figure 8 shows an orientational trajectory that exhibits large deviations after reverting the flow. The orientational motion is at first retraced, but after the rod has retraced a full flip, deviations in the orientational motion become noticeable and continue to grow rapidly.

4 Discussion

Figures 6, 7, and 8 show both translational and orientational trajectories of rods advected in a channel flow. The translational trajectories indicate that the experiment is successfully controlled: the rods stay on straight streamlines during the whole experiment in Figs. 6, 7, and 8. On a finer scale, we see that the streamline followed by the centre of mass is slightly curved, on the order of 10 μm . This is probably due to imperfections in the channel walls. After reversal, the centre-of-mass trajectories of the rods follow the streamlines very well, with only minor fluctuations on the order of one micrometre.

Our main results are the orientational trajectories of the rods shown in Figs. 6, 7, and 8. As expected, we observe tumbling motion and the results include both periodic tumbling (Figs. 6, 7) and aperiodic tumbling (Fig. 8). Different realisations of the experiment result in different tumbling periods. Moreover, we observe a weak phase drift between trajectories before and after reversal.

We discuss these observations by first briefly recalling the hydrodynamic theory of Jeffery [11] and its implications for both axisymmetric and triaxial rods. The theory is valid when the difference in flow velocity at different ends of the rod is well approximated by the flow gradient. In our experiment, this is the case because the length of the rods (30 μm) is much smaller than the smallest channel dimension of 400 μm (see also Fig. 2).

Small axisymmetric rods suspended in a shear flow tumble periodically. More precisely, the orientation vector follows one of infinitely many possible periodic Jeffery orbits. Which particular orbit the rod takes is determined by its initial orientation. For most Jeffery orbits, the rod tumbles: it stays aligned with the streamline for most of the time, but at times it rapidly flips by 180° . When the initial orientation of the rod is very close to the vorticity direction, the tumbling is less pronounced. The corresponding type of orientational motion is often referred to as “kayaking” in the literature, owing to its similarity to the motion of a kayak paddle.

For Jeffery orbits, the tumbling period does not depend on the initial orientation of the rod. The period for a rod of aspect ratio λ suspended in a shear flow of strength s is given by

$$T_{\text{Jeffery}} = \pi \frac{\lambda^2 + 1}{s\lambda}. \quad (3)$$

As mentioned in the introduction, asymmetric rods also tumble, but not necessarily in a periodic fashion [10,20].

We begin the discussion of Figs. 6 and 7 by noting two consequences of Eq. (3). First, this equation shows that the different tumbling periods in Figs. 6 and 7 can result from differences in aspect ratio or shear strength: larger aspect ratios correspond to longer periods and stronger shear to shorter periods. The lengths of the rods shown in Figs. 6 and 7 are approximately the same. But the resolution of our microscope does not allow us to precisely determine the thickness of the two rods. We cannot exclude that the different tumbling periods are in part caused by different aspect ratios of the two rods.

Second, we discuss the phase drift between the forward and backward orientational trajectories seen in Figs. 6 and 7 in terms of Eq. (3). We argue that the phase drift is due to fluctuations in the shear that are caused by small fluctuations of the y -coordinate of the centre-of-mass position. As explained in Sect. 2.1, the shear is a function of the y -coordinate. Our experimental set-up does not allow us to measure fluctuations in the y -coordinate, but if we assume that the centre-of-mass drift in y is similar in magnitude to that in z (on the order of a few micrometres), we can find a lower bound for the expected phase drift as follows. According to Eq. (3), the period is inversely proportional to the shear strength. It follows that the relative change in shear strength equals the relative change in time between flips, $\Delta s/s = \Delta T/T$. The flow profile in the y -direction is approximately a quadratic function, $u_x = -\alpha y^2$, which implies that $\Delta T/T = \Delta y/y$. Equating y with the channel depth (400 μm) allows us to estimate that the drift should at least be 1 %, in agreement with panels (b) and (c) in Figs. 6 and 7.

We conclude the discussion by examining the trajectory in Fig. 8. We see, first, that the trajectory is clearly aperiodic, both before and after reversal. The numerical experiments by Yarin et al. [20] indicate that triaxial rods may exhibit aperiodic dynamics even for very small deviations from axisymmetry (that could not be resolved by our microscope). Secondly, the forward and backward orientational trajectories in panel (c) of Fig. 8 separate rapidly. In fact, the trajectory appears at first to reverse perfectly but then the difference between forward and backward orientational trajectories grows substantially. These observations suggest that Fig. 8 corresponds to chaotic tumbling of a triaxial particle.

5 Conclusions

We have designed a microfluidic set-up with video microscopy and tracking software to measure the translational and orientational trajectories of microrods advected in microchannel flows. The experiments presented here demonstrate the level of control and accuracy of the current set-up. We observe both periodic and aperiodic (and possibly chaotic) orientational dynamics.

Further work on the experiment aims to improve the efficiency and capability of the current set-up. For example, we plan to install an optical tweezer in order to control initial orientations of the rods. This would make it possible to observe different orientational behaviours (such as those shown in Figs. 6 and 8) for *the same* rod.

Acknowledgements Financial support from the Swedish Research Council, the Göran Gustafsson Foundation for Research in Natural Sciences and Medicine, and the European COST action MP0806 is gratefully acknowledged.

References

1. Alargova, R., Bhatt, K., Paunov, V., Velev, O.: Scalable synthesis of a new class of polymer microrods by a liquid-liquid dispersion technique. *Adv. Mater.* **16**(18), 1653–1657 (2004)
2. Bezuglyy, V., Mehlig, B., Wilkinson, M.: Poincaré indices of rheoscopic visualisations. *Europhys. Lett.* **89**(3), 34003 (2010)
3. Brenner, H.: Rheology of a dilute suspension of axisymmetric Brownian particles. *Int. J. Multiph. Flow* **1**(2), 195–341 (1974)
4. Brody, J., Yager, P., Goldstein, R., Austin, R.: Biotechnology at low Reynolds numbers. *Biophys. J.* **71**(6), 3430–3441 (1996)
5. Canny, J.: A computational approach to edge detection. *IEEE Trans. PAMI Pattern Anal. Mach. Intell.* **8**(6), 679–698 (1986)
6. Cheng, N.-S.: Formula for the viscosity of a glycerol-water mixture. *Ind. Eng. Chem. Res.* **47**(9), 3285–3288 (2008)
7. Goldsmith, H., Mason, S.: The flow of suspensions through tubes. I. Single spheres, rods, and discs. *J. Colloid Sci.* **17**(5), 448–476 (1962)
8. Halř, R., Flusser, J.: Numerically stable direct least-squares fitting of ellipses. In: *Proceedings of the 6th International Conference in Central Europe on Computer Graphics and Visualization*. pp. 125–132 (1998)
9. Hinch, E.J., Leal, L.G.: The effect of Brownian motion on the rheological properties of a suspension of non-spherical particles. *J. Fluid Mech.* **52**(04), 683–712 (1972)

10. Hinch, E.J., Leal, L.G.: Rotation of small non-axisymmetric particles in a simple shear flow. *J. Fluid Mech.* **92**(03), 591–607 (1979)
11. Jeffery, G.B.: The motion of ellipsoidal particles immersed in a viscous fluid. *Proc. R. Soc. Lond. Ser. A* **102**(715), 161–179 (1922)
12. Kaya, T., Koser, H.: Characterization of hydrodynamic surface interactions of *Escherichia coli* cell bodies in shear flow. *Phys. Rev. Lett.* **103**, 138103 (2009)
13. Mishra, Y.N., Einarsson, J., John, O.A., Andersson, P., Mehlig, B., Hanstorp, D.: A microfluidic device for the study of the orientational dynamics of microrods. vol. 8251. SPIE, p. 825109 (2012)
14. Ott, E.: *Chaos in Dynamical Systems*. Cambridge University Press, Cambridge (1993)
15. Parsa, S., Calzavarini, E., Toschi, F., Voth, G.A.: Rotation rate of rods in turbulent fluid flow. *Phys. Rev. Lett.* **109**, 134601 (2012)
16. Petrie, C.J.: The rheology of fibre suspensions. *J. Non-Newton. Fluid Mech.* **87**(2–3), 369–402 (1999)
17. Wilkinson, M., Bezuglyy, V., Mehlig, B.: Fingerprints of random flows? *Phys. Fluids* **21**(4), 043304 (2009)
18. Wilkinson, M., Bezuglyy, V., Mehlig, B.: Emergent order in rheoscopic swirls. *J. Fluid Mech.* **667**, 158–187 (2011)
19. Wilkinson, M., Kennard, H.R.: A model for alignment between microscopic rods and vorticity. *J. Phys. A: Math. Theor.* **45**, 455502 (2012)
20. Yarin, A., Gottlieb, O., Roisman, I.: Chaotic rotation of triaxial ellipsoids in simple shear flow. *J. Fluid Mech.* **340**, 83–100 (1997)